

Effects of heating strategies and ballistic transport on the transient thermal conduction in 3D FinFETs

Chuang Zhang^a, Ziyang Xin^b, Qin Lou^c, Hong Liang^{a,*}

^aDepartment of Physics, School of Sciences, Hangzhou Dianzi University, Hangzhou 310018, China

^bSchool of Energy and Power Engineering, Huazhong University of Science and Technology, Wuhan, 430074, China

^cSchool of Energy and Power Engineering, University of Shanghai for Science and Technology, Shanghai 200093, China

Abstract

Efficiently capturing the three-dimensional spatiotemporal distributions of temperature is of great significance for alleviating hotspot issues in 3D FinFETs. However, most previous thermal simulations mainly focused on the steady-state problem with continuous heating. Few studies are conducted for the transient thermal conduction in 3D FinFETs with non-continuous heating, which is actually closer to the reality. To investigate the effects of heating strategies on the transient micro/nano scale thermal conduction in 3D FinFETs, three heating strategies are considered, including ‘Continuous’, ‘Intermittent’ and ‘Alternating’ heating. A comparison is made between the phonon BTE solutions and the data predicted by the macroscopic diffusion equation, where the effect of boundary scattering on phonon transport is added into the effective thermal conductivity. Numerical results show that it is not easy to accurately capture the heat conduction in 3D FinFETs by the macroscopic diffusion equation, especially near the hotspot areas where ballistic phonon transport dominates and the temperature diffusion is no longer valid. Different heating strategies have great influence on the peak temperature rise and transient thermal dissipation process. Compared to ‘Intermittent’ or ‘Continuous’ heating, the temperature variance of ‘Alternating’ heating is smaller.

Keywords: Micro/nano scale heat conduction, Fin field-effect transistors, Hotspot issues, Boltzmann transport equation, Discrete unified gas kinetic scheme

1. INTRODUCTION

Advanced process technologies represented by Fin field-effect transistors (FinFETs) continue to promote the development of the semiconductor and microelectronics industries [1, 2, 3, 4]. However, when the number density, heat generation power and heat flux density of transistors increases sharply, the hotspot problem becomes increasingly serious, threatening the safe operation of electronic devices [5, 6, 7]. As a mainstream structure in logic chips or semiconductor devices, single three-dimensional FinFET unit has geometric dimensions ranging from tens of nanometers to hundreds of nanometers. This size scale is comparable to the phonon mean free path of room temperature silicon, so that the classic Fourier law of heat conduction no longer holds [8, 9, 10, 11]. Therefore, it is very important to understand the micro/nano scale heat transfer physics and efficiently predict the three-dimensional temporal and spatial distributions of temperature in order to alleviate the hotspot problem in microelectronics [12, 13, 14, 15, 16].

A mainstream engineering treatment method is to adopt a 3D heat diffusion equation with an effective thermal conductivity which takes into account the size effect [14, 15, 17, 12, 18, 19,

20]. This method is widely used in many industrial softwares such as TCAD, ANSYS and COMOSL. These softwares contain huge material databases, so that the users can select the appropriate thermal conductivity coefficient based on the material components, size, temperature, doping concentration, etc. This also indicates that its numerical accuracy significantly depends on the engineers’ experience. The disadvantage is that it still assumes a linear relationship between the heat flux and temperature gradient. To solve this drawback, many macroscopic moment equations [21, 22, 23, 24, 9] have been developed by introducing time delay terms, memory effects, heat flux nonlinearity or nonlocal terms, that is, introducing high-order derivatives or tensors of temperature and heat flux with respect to time and space. These non-Fourier heat conduction models can capture non-equilibrium or non-diffusive effects to some extent. However, a small parameter expansion assumption is usually adopted during derivation process, so that it is difficult for most of them to accurately characterize ballistic transport, especially in complex 3D geometries.

Another accessible method is to numerically solve the mesoscopic phonon Boltzmann transport equation (BTE) [25, 12, 26, 27]. Adisusilo, *et al* used the Monte Carlo method to simulate the thermal properties of a 3D bulk FinFET with gate length 22 nm and fin thickness 8 nm. Numerical results show that the peak temperature predicted by classical Fourier’s law is 100 K lower than that of Monte Carlo method. Hu, *et al* [28] and Zhang, *et al* [19] used the synthetic iterative scheme to capture

*Corresponding author

Email addresses: zhangc520@hdu.edu.cn (Chuang Zhang), xinzhiyang@hust.edu.cn (Ziyang Xin), louqin560916@163.com (Qin Lou), lianghongstefanie@163.com (Hong Liang)

non-equilibrium thermal conduction in 3D bulk FinFET. Numerical results show that the peak temperature rise in FinFET predicted by the phonon BTE deviates from those predicted by the macroscopic diffusion equation even if an effective thermal conductivity is used [19].

The phonon BTE is usually regarded as the core bridge in connecting microscopic or macroscopic methods in many multi-scale thermal simulation [29]. For instance, the IMEC research team [30, 15, 14] used the modular method to evaluate the thermal performance of the back-end of line. They calculated the thermal physical parameters of electrons and phonons using the first principles as the input parameters of BTE, and then used the Monte Carlo method to numerically solve the BTE and extracted the effective thermal conductivity of materials such as nanoscale interconnects and through-holes. Finally, the macroscopic diffusion equation is solved to extract the effective thermal resistance of each layer of back-end of line in a reasonable calculation time. The Intel research team [12, 18] numerically solves the phonon BTE to obtain the effective thermal conductivity of the entire silicon fin or nanowires, where the heat source term is obtained from electron-phonon coupling. After that, a larger thermal simulations at the cell or circuit level is conducted to assess the effects of self-heating on interconnects and circuits by numerically solving the macroscopic equation.

In the above studies of heat dissipation in FinFETs [31, 32, 18, 15, 33], a continuous heating source is usually used and steady-state temperature field is analyzed. However, the electronic equipments do not always work and the transient thermal evolution process is much more noteworthy in reality [34, 12, 35]. In this paper, the effects of heating strategies on the transient thermal conduction in FinFET are investigated based on the phonon BTE. Three heating strategies are accounted and the associated steady or unsteady thermal dissipations processes are simulated, analyzed and discussed. The rest of this article is organized as follows. Theoretical models and methods are introduced briefly in Sec. 2. Results and discussions for the heat dissipation in FinFETs are conducted in Sec. 3. Finally, conclusion and outlook are made in Sec. 4.

2. MODELS

The phonon BTE under the single-mode relaxation time approximation (RTA) is used to describe the phonon transport in FinFETs [36, 25, 37, 37, 38, 26, 27, 18, 39],

$$\frac{\partial f}{\partial t} + v_g \mathbf{s} \cdot \nabla_{\mathbf{x}} f = \frac{f^{eq} - f}{\tau} + \frac{1}{4\pi} \dot{S}, \quad (1)$$

where $f = f(\mathbf{x}, \mathbf{s}, t)$ is the phonon distribution function of energy density, which depends on spatial position \mathbf{x} , unit directional vector \mathbf{s} and time t . f^{eq} is the associated equilibrium distribution function, v_g is the phonon group velocity, τ is the relaxation time and $\dot{S} = \dot{S}(\mathbf{x}, t)$ is the external heat source. Taking an integral of Eq. (1) over the solid angle space $d\Omega$ leading to the first law of thermodynamics with energy U and heat flux

\mathbf{q} ,

$$\frac{\partial U}{\partial t} + \nabla_{\mathbf{x}} \cdot \mathbf{q} = \int \frac{f^{eq} - f}{\tau} d\Omega + \dot{S} = \dot{S}, \quad (2)$$

$$U = \int f d\Omega = CT, \quad \mathbf{q} = \int v_g \mathbf{s} f d\Omega. \quad (3)$$

where C is the specific heat and T is the temperature. The phonon scattering kernel satisfies energy conservation,

$$\int \frac{f^{eq} - f}{\tau} d\Omega = 0. \quad (4)$$

Silicon and silicon dioxide are two main semiconductor materials in FinFETs, and their thermal properties at room temperature 300 K can be obtained from previous references [40, 41, 42], as listed in Table. 1.

Table 1: Thermal properties of room temperature silicon (Si) and silicon dioxide (SiO₂) [40, 41, 42].

	C (J·m ⁻³ ·K ⁻¹)	v_g (m·s ⁻¹)	λ (nm)
Si	1.5E6	3.0E3	100.0
SiO ₂	1.75E6	5.9E3	0.4

Discrete unified gas kinetic scheme (DUGKS) [36, 43] is used to solve the phonon BTE accounted for the interfacial thermal resistance [44, 45, 46, 17]. Detailed introductions and numerical settings can be found in Appendix A and Appendix B. Note that the numerical discrete solution of the seven-dimensional phonon BTE requires extremely high computing resources and cost. Hence, the isotropic wave vector and frequency-independence assumption is used in the present paper to achieve a good balance between computational efficiency and accuracy. All numerical simulations are conducted by a home-made C/C++ program [43, 35].

3. RESULTS AND DISCUSSIONS

Motivated by previous thermal simulations of 3D FinFET [33, 47, 18, 32, 19] based on the phonon BTE, we only investigate the three-dimensional transient phonon conduction problem in single or several FinFETs in this paper. Schematics of 3D bulk or SOI FinFETs are shown in Fig. 1, both of which are composed of silicon fin, silicon dioxide insulation layer and silicon substrate with several contact interfaces. The system sizes in the x , y , z direction of a single FinFET are 28nm, 56 nm and 82 nm, respectively. Front, back, left and right surfaces are all symmetric boundaries. The whole diagram is geometrically symmetric in the x and y directions with respect to the purple dot dash lines. Bottom surfaces are the heat sink with fixed environment temperature and the other surfaces are all diffusely reflecting adiabatic boundaries. The heat source is located in the fin area, whose system size in the x , y , z direction are 8, 10 and 32 nm, respectively. The entire structure size is approximately a 7 nm technology node transistor.

Three heating strategies are mainly considered, where ‘Continuous’ represents that the two external heat sources always

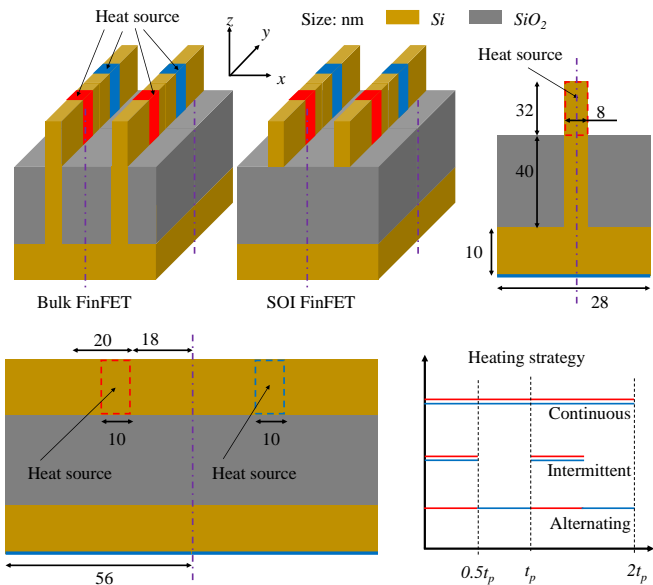


Figure 1: Three-dimensional global graph of four bulk or silicon-on-insulator (SOI) FinFETs. For the red and blue heat source areas in 3D FinFETs, the following three heating strategies are used, including ‘Continuous’, ‘Intermittent’, ‘Alternating’, where t_p is a heating period.

heat the system. It indicates a steady heat source, which is used in most previous papers. ‘Intermittent’ represents that the two external heat sources work together and both of them heat the system in a half time. It is a bit like the heating method in pump-probe experiments, where the heat source heats the system for a while and does not heat it for a while. ‘Alternating’ represents that the two external heat sources work alternatively and each one heats the system in a half time, where t_p is a heating period. It is much like the N and P type transistors in chips are periodically arranged on the substrate and interlace to work when the AC voltage is loaded. For typical chips in electronic devices (e.g., laptop), the working frequency is about 4 GHz so that we set $t_p = 0.25$ ns. The maximum heating power is $5.0 \times 10^{16} \text{ W}\cdot\text{m}^{-3}$. The temperature dependence of phonon thermophysical parameters [43, 19] is not accounted, therefore, the predicted temperature rise is basically linear to the input power density based on dimensionless analysis of the phonon BTE [36].

A lot of previous experimental or theoretical work has proven the failure of classical Fourier’s law at the micro/nano scale [10, 48, 49, 11], so we focus on comparing the BTE results with the macroscopic diffusion equation with empirically modified effective thermal conductivity coefficients [14, 15, 17, 12, 18, 19, 20], namely, effective Fourier’s law (EFL). Detailed introductions and numerical discretizations can be found in Appendix C.

Firstly, steady-state temperature fields in bulk or SOI FinFET are simulated and compared in Fig. 2 with ‘continuous heating’. It can be found that the deviations of temperature fields in the whole domain between the BTE and EFL are smaller in SOI FinFET than those in bulk FinFET. The underlying physical mechanisms can be explained from the perspective of mate-

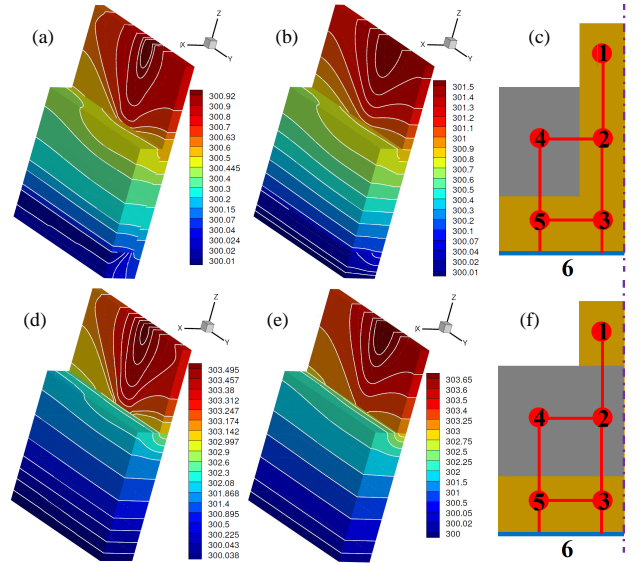
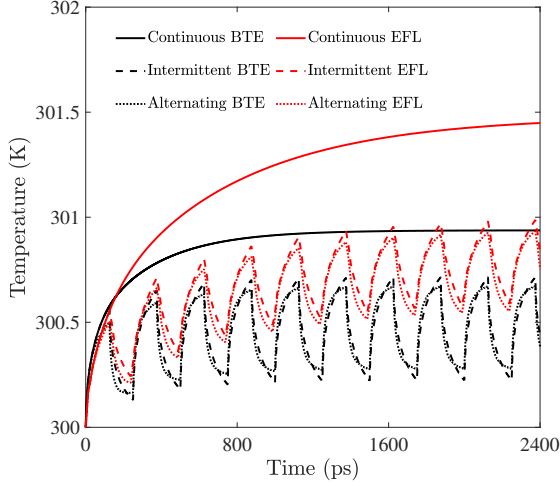


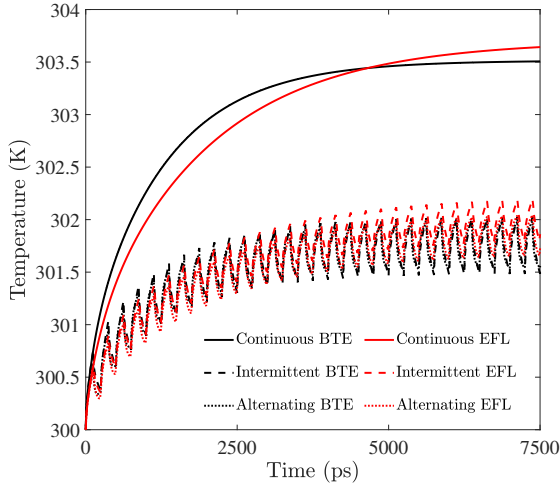
Figure 2: The first two column are the steady temperature contour of a half of FinFET under ‘Continuous’ heating. The last column is the schematic of heat dissipation path from the heat source to heat sink in the XZ plane. (a,b,c) Bulk FinFET. (d,e,f) SOI FinFET. (a,d) BTE. (b,e) EFL.

rial composition and phonon transport properties. Schematics of heat dissipation paths in bulk FinFET and SOI FinFET are shown in Fig. 2(c) and (f), respectively, where there is thermal resistance in the channels between two nodes. In SOI FinFET (Fig. 2(f)), phonons must pass through two Si/SiO₂ interfaces and the silicon dioxide region when they need to transport thermal energy from the heat source region to the heat sink region. On one hand, the small phonon mean free path in silicon dioxide leads to a diffusive transport, where the EFL is valid. On the other hand, two Si/SiO₂ interfaces significantly increases the thermal resistance and decreases the heat dissipation efficiency. As shown in Fig. 2(d,e), the temperature gradient is basically along the z direction and the temperature variance presents a linear distribution in the silicon dioxide and bottom silicon substrate areas. On the contrary, phonons can transfer energy directly from the heat source region to the bottom heat sink only through the silicon material in the bulk FinFET after absorbing a large amount of energy from the heat source, namely, heat dissipation path 1 – 2 – 3 – 6 in Fig. 2(c). In this process, ballistic transport dominates the heat conduction. Although a lower effective thermal conductivity is introduced in the EFL, the linear assumption between the heat flux and temperature gradient still leads to some deviations compared to the results of phonon BTE. If we consider the nonlinear, nonlocal, time delay or memory effects in the macroscopic equation, the deviation between the macroscopic simulations and the phonon BTE may be smaller.

In addition, the temperature fields in bulk FinFET predicted by phonon BTE in the bottom silicon substrate areas (Fig. 2a) are completely different from those predicted by EFL (Fig. 2b). Actually it is a competition result of two heat transfer channels with different heat transfer efficiency and various phonon transport behaviors, which can be explained according to the



(a) Bulk FinFET



(b) SOI FinFET

Figure 3: Transient evolutions of the maximum temperature in the 3D hotspot system under three heating strategies.

heat dissipation channel 2 – 4 – 5 and 2 – 3 – 5 in Fig. 2(c). In heat dissipation channel 2 – 4 – 5, on one hand, two interfacial thermal resistance exists in the thermal transport process from 2 to 4 and from 4 to 5. On the other hand, the phonon mean free path of silicon dioxide is much smaller than 8 nm. In heat dissipation channel 2 – 3 – 5, the transfer of thermal energy only happens in the silicon materials without interfacial thermal resistance and ballistic phonon transport dominates heat conduction. Compared to channel 2 – 3 – 5, there is larger thermal resistance and lower phonon transport efficiency in channel 2 – 4 – 5. Hence, it can be found that the temperature contour line in bottom silicon areas is even perpendicular to the bottom surface. When using the EFL, ballistic phonon transport in heat dissipation channel 2 – 3 – 5 is replaced by the temperature diffusion with an effective thermal conductivity. It is well known that one of the drawbacks of the diffusion equation is that it has an infinite heat propagation speed [22], namely, the effect of a temperature fluctuation or change at any spatial point can instantly affect the entire region. Hence, it can be found that the

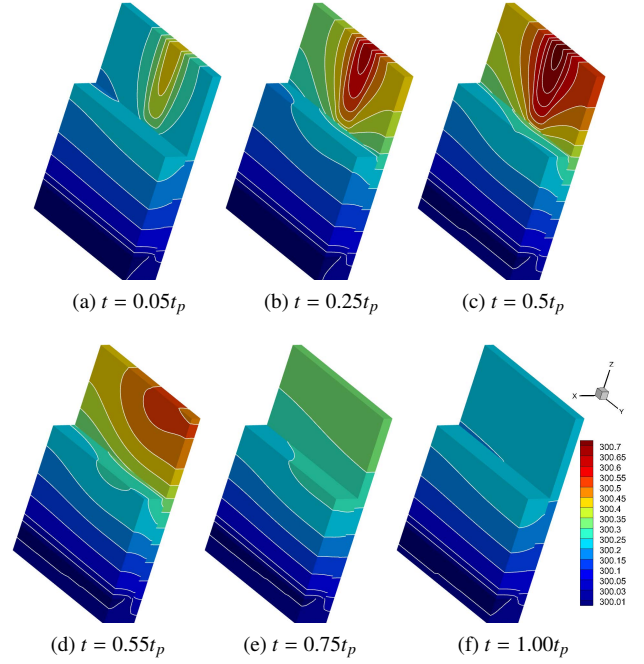


Figure 4: Transient temperature contour of a half of bulk FinFET predicted by BTE under ‘Intermittent’ heating when the system reaches the periodic steady state.

temperature contour line mainly parallel to the bottom surface.

Secondly, the evolution of transient peak temperature over time in bulk or SOI FinFET under three heating strategies is shown in Fig. 3. The temperature predicted by EFL rises more slowly than BTE at the initial stage, and it also takes longer to reach the periodic steady state. When the system reaches the periodic steady state, the transient temperature predicted by EFL is also inconsistent with the BTE results. For example, the ‘Intermittent’ heating has a higher peak temperature rise than that of ‘Alternating’ heating in the heating stage and has a lower peak temperature in the second half of the heating period in the BTE solutions. However, in the EFL prediction results, the maximum temperature of the ‘Alternating’ heating is lower than that of the ‘Intermittent’ heating in the second half of the heating period. Compared to ‘Intermittent’ heating, the temperature variance of ‘Alternating’ heating is smaller.

Thirdly, the transient heat dissipation process in bulk or SOI FinFET under ‘Intermittent’ or ‘Alternating’ heating is described. The temperature contour predicted by BTE at different moments is plotted when the system reaches the periodic steady state in Figs. 4 to 7, where $t = 0.25t_p$ represents that the current moment is a quarter of a heating period. The periodic steady state represents that the temporal and spatial distributions of the temperature field in the current heating period is the same as those in the next heating period, with a relative deviation of less than 10^{-6} .

In bulk FinFET under ‘Intermittent’ heating, when the external heat source begins to heat the system, e.g., $t = 0.05t_p$, the temperature near the heat source areas begins to rise continuously, and the high thermal energy in the fin region is rapidly

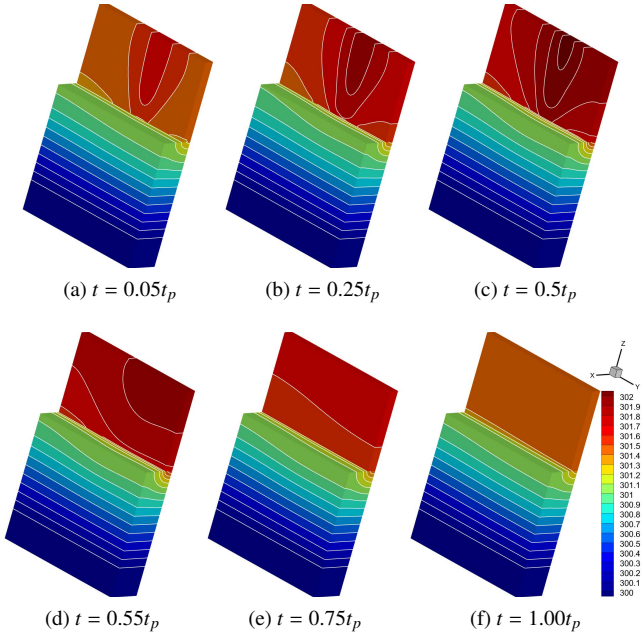


Figure 5: Transient temperature contour of a half of SOI FinFET predicted by BTE under ‘Intermittent’ heating when the system reaches the periodic steady state.

transferred from hotspot area to other geometric regions by phonon ballistic transport. At the contact interface between the silicon fin and the silicon dioxide insulation layer, the temperature in the silicon region is higher than that of the silicon dioxide region at the same z height. However, when $t = 0.25t_p$ or $t = 0.5t_p$, the temperature in the silicon region is lower than that of the silicon dioxide region at the same z height. This is because the mean free path or thermal diffusivity rate of silicon is much higher than that of silicon dioxide, which leads to a higher heat dissipation efficiency. The thermal energy in silicon dioxide is mainly transferred from silicon to silicon dioxide through the interface, and then transferred to the bottom heat sink. As shown in Fig. 2(c), the heat dissipation efficiency of channel 2 – 3 – 6 is much higher than that of 2 – 4 – 5 – 6. Although the thermal energy is transferred from silicon to silicon dioxide through the interface at the beginning $t = 0.05t_p$, the energy in silicon dioxide is not efficiently transferred to the bottom heat sink due to its small mean free path, small thermal diffusivity and large interfacial thermal resistance. It is similar to a thermal reservoir. Over time, the silicon dioxide region actually got hotter, even higher than that of silicon at the same z height. When the heat source is removed $t > 0.5t_p$, the peak temperature decreases significantly due to the large mean free path of silicon.

In SOI FinFET under ‘Intermittent’ heating, it is well known that the silicon dioxide insulation layer is mainly introduced to improve electrical performance in the actual chip design [1, 50], but inevitably, it increases the temperature of silicon fin area due to low thermal conductivity. From Fig. 5, it can be observed that the temperature of the silicon fin region changes dramatically with time in a heating period, which actually generates a

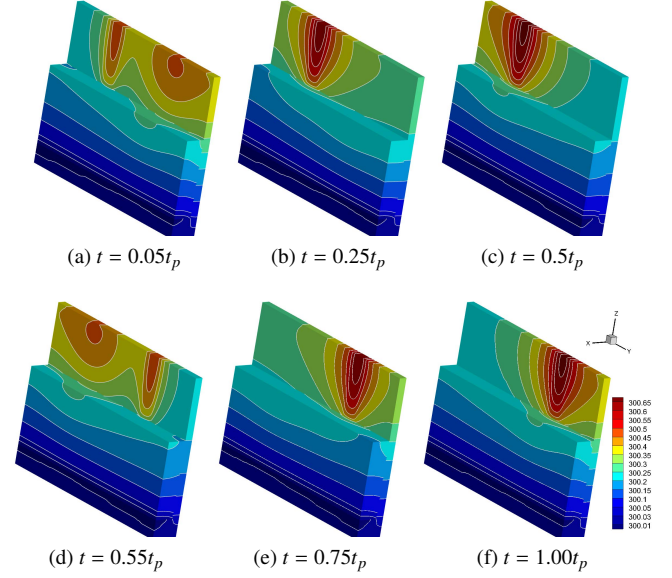


Figure 6: Temperature contour of bulk FinFET at different moments predicted by BTE under ‘Alternating’ heating when the system reaches the periodic steady state.

large thermal shock to the materials. Oppositely, the temperature contour profiles in the silicon dioxide insulation layer and silicon substrate region are basically flat, showing a linear distribution. In other words, the silicon dioxide insulation layer reduces the thermal shock on the bottom substrate material although it raised the overall temperature in the fin area.

For ‘Alternating’ heating, two external heat source heat the system in turn so that the thermal conduction characteristics in the y direction are no longer symmetrical. Temperature contour in bulk or SOI FinFET at different moments under ‘Alternating’ heating when the system reaches the periodic steady state is plotted in Figs. 6 and 7. When $t \leq 0.5t_p$, one heat source starts to provide thermal energy so that the hotspot temperature increases, while the other is removed so that the hotspot temperature decreases gradually. Therefore, compared to the ‘Intermittent’ heating in Figs. 4 and 5, we can see that there is always a high temperature hotspot in the silicon fin region. This actually reflects that the overall temperature in the silicon fin region under ‘Alternating’ heating fluctuates less over time than that of under ‘Intermittent’ heating, which is also verified in Fig. 3. Less temperature fluctuations represents smaller thermal shock on materials, which could delay the material life to some extent.

4. CONCLUSION

Steady/unsteady heat dissipation in nanoscale bulk or SOI transistors under different heating strategies is investigated by the phonon BTE. Results show that it is not easy to accurately capture the heat conduction in transistors by the EFL although the effect of boundary scattering on phonon transport is added into the effective thermal conductivity. There are still some deviations between the results of phonon BTE and EFL, espe-

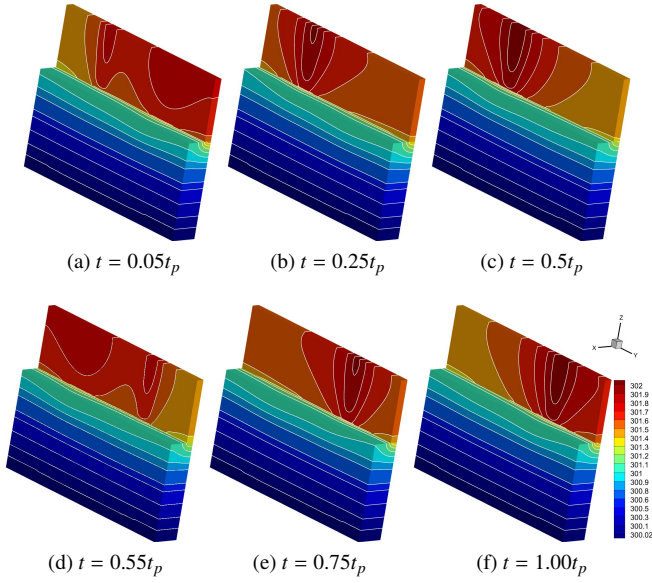


Figure 7: Temperature contour of SOI FinFET at different moments predicted by BTE under ‘Alternating’ heating when the system reaches the periodic steady state.

cially near the hotspot areas where ballistic phonon transport dominates and the temperature diffusion is no longer valid. Although the silicon dioxide increases the peak temperature significantly, it makes the temperature profiles in the silicon dioxide insulation layer and silicon substrate region flat, which reduces the dramatic temperature fluctuations. Different heating strategies have great influence on the peak temperature rise and transient thermal dissipation process. Compared to ‘Intermittent’ or ‘Continuous’ heating, the temperature variance of ‘Alternating’ heating is smaller, which indicates that this heating strategy also reduces the dramatic temperature fluctuations.

Acknowledgment

Q.L. acknowledges the support of the National Natural Science Foundation of China (52376068). C.Z. acknowledges the members of online WeChat Group: Device Simulation Happy Exchange Group, for extensive discussions. The authors acknowledge Beijing PARATERA Tech CO.,Ltd. for providing HPC resources that have contributed to the research results reported within this paper.

Appendix A. Discrete unified gas kinetic scheme

The interfacial thermal resistance R_{eff} between two dissimilar solid materials is [45, 44]

$$R_{eff} = \frac{\delta T}{q}, \quad (\text{A.1})$$

where δT and q are the temperature drop between the two sides of the interface and the heat flux across the interface, respectively. In order to deal with the interfacial thermal resistance

between silicon and silicon dioxide materials, the diffuse mismatch model is used [44, 45, 46, 17], which assumes that all phonons loses previous memories and completely follows the diffuse transmitting or reflecting rule after interacting with the interface. Transmittance and reflectance on each side of the interface satisfy

$$r_{12} + t_{12} = 1 \quad (\text{A.2})$$

due to energy conservation, where t_{12} (or t_{21}) represents the transmittance from medium 1 (or medium 2) to medium 2 (or medium 1) across the interface, and r_{12} (or r_{21}) represents the reflectance in the medium 1 (or medium 2) reflected back from the interface. Note that the net heat flux across the interface should be zero at the thermal equilibrium state due to the principle of detailed balance so that

$$t_{12}C_1v_1 = t_{21}C_2v_2, \quad (\text{A.3})$$

where C_1 and v_1 (or C_2 and v_2) are the specific heat and group velocity of medium 1 (or medium 2).

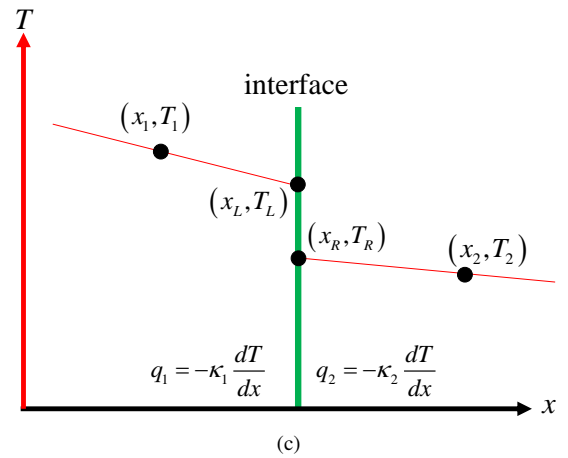
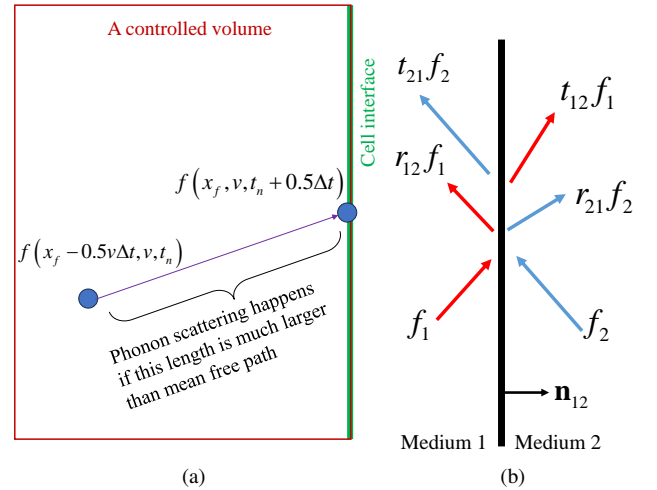


Figure A.8: (a) Reconstruction of phonon distribution function at the cell interface for a given discretized controlled volume. (b) Transmittance and reflectance of phonon distribution function on each side of the interface between medium 1 and medium 2. (c) Schematic of the spatial distributions of temperature near the interface between medium 1 and medium 2.

Discrete unified gas kinetic scheme (DUGKS) is used to solve the transient frequency-independent phonon BTE. More specific numerical solution process and boundary treatments can be found in previous papers [36, 51]. Here we make a brief introduction of DUGKS. Under the discretized six-dimensional phase space, the phonon BTE is

$$\begin{aligned} & \frac{f_{i,k}^{n+1} - f_{i,k}^n}{\Delta t} + \frac{\Delta t}{V_i} \sum_{j \in \mathcal{N}(i)} (v_g \mathbf{s}_k \cdot \mathbf{n}_{ij} f_{ij,k}^{n+1/2} S_{ij}) \\ & = \frac{\Delta t}{2} (H_{i,k}^{n+1} + H_{i,k}^n), \end{aligned} \quad (\text{A.4})$$

where i, k, ij, n are the indexes of cell center, solid angle, cell interface and time step at the finite-volume discrete level, respectively. $H = (f^{eq} - f)/\tau + \dot{S}/(4\pi)$. In order to update the phonon distribution function from $f_{i,k}^n$ to $f_{i,k}^{n+1}$, the key is the reconstruction of the distribution function at the cell interface at the half time step $f_{ij,k}^{n+1/2}$. When a phonon is transferred from the inner region of a control volume to the interface after half a time step, it will suffer a large number of phonon scattering processes if the time step is much longer than the phonon relaxation time or this length is much larger than mean free path, as shown in Fig. A.8(a). To respect this physical law, the phonon BTE is solved again along the direction of group velocity and trapezoidal quadrature is used for the time integration of the scattering terms,

$$\begin{aligned} & f(\mathbf{x}_f, \mathbf{v}, t_n + 0.5\Delta t) - f(\mathbf{x}_1, \mathbf{v}, t_n) \\ & = \frac{\Delta t}{4} (H(\mathbf{x}_f, t_n + 0.5\Delta t) + H(\mathbf{x}_1, t_n)) \end{aligned} \quad (\text{A.5})$$

$$\implies \bar{f}(\mathbf{x}_f, \mathbf{v}, t_n + 0.5\Delta t) = \bar{f}^+(\mathbf{x}_1, \mathbf{v}, t_n), \quad (\text{A.6})$$

where \mathbf{x}_f is the center of cell interface, $\mathbf{x}_1 = \mathbf{x}_f - 0.5\mathbf{v}\Delta t$, $\bar{f} = f - \frac{\Delta t}{4}H$, $\bar{f}^+ = f + \frac{\Delta t}{4}H$. Equations (A.4) and (A.5) are the key evolution process of DUGKS [36], that is, solving the discrete BTE at the cell center in a complete time step, while coupling phonon advection and scattering together in the reconstruction of the interfacial distribution function at the half time step, through which it allows the time step or cell size to be much larger than the relaxation time and phonon mean free path in the (near) diffusive regime. The phonon distribution function incident into the cell interface is

$$f(\mathbf{x}_f) = \frac{4\tau}{4\tau + \Delta t} \left(\bar{f}(\mathbf{x}_f) + \dot{S}/(4\pi) + \frac{\Delta t}{4\tau} f^{eq}(\mathbf{x}_f) \right), \quad (\text{A.7})$$

from which it can be found that we have to firstly calculate the equilibrium state at the cell interface $f^{eq}(\mathbf{x}_f)$ if we want to reconstruct the distribution function $f(\mathbf{x}_f)$ based on $\bar{f}(\mathbf{x}_f)$.

Here we focus on how to reconstruct the transmission and reflection distribution function at the interface between two dissimilar solid materials. As shown in Fig. A.8(b), the phonon transmission and reflection at the interface are related to the phonon distribution on both sides. Diffuse mismatch model assumes that the phonon distribution at the interface pointing from interface to medium 1 (or medium 2) follows the equilib-

rium distribution with temperature T_1^p (or T_2^p). Then we have

$$\begin{aligned} & \int_{\mathbf{v}_1 \cdot \mathbf{n}_{12} > 0} -r_{12} f_1 \mathbf{v}_1 \cdot \mathbf{n}_{12} d\Omega + \int_{\mathbf{v}_2 \cdot \mathbf{n}_{12} < 0} t_{21} f_2 \mathbf{v}_2 \cdot \mathbf{n}_{12} d\Omega \\ & = \int_{\mathbf{v}_1 \cdot \mathbf{n}_{12} < 0} f^{eq}(T_1^p) \mathbf{v}_1 \cdot \mathbf{n}_{12} d\Omega \end{aligned} \quad (\text{A.8})$$

$$\begin{aligned} & \int_{\mathbf{v}_1 \cdot \mathbf{n}_{12} > 0} t_{12} f_1 \mathbf{v}_1 \cdot \mathbf{n}_{12} d\Omega + \int_{\mathbf{v}_2 \cdot \mathbf{n}_{12} < 0} -r_{21} f_2 \mathbf{v}_2 \cdot \mathbf{n}_{12} d\Omega \\ & = \int_{\mathbf{v}_2 \cdot \mathbf{n}_{12} > 0} f^{eq}(T_2^p) \mathbf{v}_2 \cdot \mathbf{n}_{12} d\Omega \end{aligned} \quad (\text{A.9})$$

$$\int_{\mathbf{v}_1 \cdot \mathbf{n}_{12} > 0} f_1 d\Omega + \int_{\mathbf{v}_1 \cdot \mathbf{n}_{12} < 0} f^{eq}(T_1^p) d\Omega = \int f^{eq}(T_1) d\Omega, \quad (\text{A.10})$$

$$\int_{\mathbf{v}_2 \cdot \mathbf{n}_{12} < 0} f_2 d\Omega + \int_{\mathbf{v}_2 \cdot \mathbf{n}_{12} > 0} f^{eq}(T_2^p) d\Omega = \int f^{eq}(T_2) d\Omega, \quad (\text{A.11})$$

$$f_1 = \frac{4\tau_1}{4\tau_1 + \Delta t} \left(\bar{f}_1 + \dot{S}/(4\pi) + \frac{\Delta t}{4\tau_1} f^{eq}(T_1) \right), \quad \mathbf{v}_1 \cdot \mathbf{n}_{12} > 0 \quad (\text{A.12})$$

$$f_2 = \frac{4\tau_2}{4\tau_2 + \Delta t} \left(\bar{f}_2 + \dot{S}/(4\pi) + \frac{\Delta t}{4\tau_2} f^{eq}(T_2) \right), \quad \mathbf{v}_2 \cdot \mathbf{n}_{12} < 0 \quad (\text{A.13})$$

where \mathbf{n}_{12} is the unit normal vector pointing from media 1 to media 2, T_1 and T_2 are the local equivalent equilibrium temperatures on each side of the interface. τ_1 (or τ_2) and \mathbf{v}_1 (or \mathbf{v}_2) are the phonon properties in medium 1 (or medium 2). The first two equations (A.8,A.9) come from the physical assumptions of diffuse mismatch model and the conservation of heat flux across the interface, for example, in Eq. (A.8), all phonons in medium 1 emitted from the interface, including the phonons in medium 1 reflecting back from the interface and the phonons in medium 2 transmitting across the interface, follow the equilibrium distribution with temperature T_1^p . T_1 (A.10) and T_2 (A.11) are calculated by taking the moment of distribution function over the whole momentum space. Combined above six equations, T_1, T_2, T_1^p and T_2^p can be obtained by Newton method.

Appendix B. Numerical discretizations and independence test

To solve the transient phonon BTE, the temporal space, solid angle space and spatial space are both discretized into a lot of small pieces. Time step is $\Delta t = 0.125$ ps and Cartesian grids with uniform cell size $\Delta x = 1$ nm is used. Solid angle $s = (\cos \theta, \sin \theta \cos \varphi, \sin \theta \sin \varphi)$ is discretized into $N_\theta \times N_\varphi = 48 \times 48$ pieces, where $\cos \theta \in [-1, 1]$ is discretized by N_θ -point Gauss-Legendre quadrature and $\varphi \in [0, \pi]$ (due to symmetry) is discretized by the Gauss-Legendre quadrature with $N_\varphi/2$ points. All numerical results are obtained by a three-dimensional C/C++ program. MPI parallelization computation with 48 CPU cores based on the decomposition of solid angle space is implemented and the discrete solid angles corresponding to the specular reflection are ensured in the same CPU core.

Take the heat conduction in 3D bulk FinFET (Fig. 1) as an example, we conduct an independent verification of the number of discrete solid angles. Steady temperature contour or heat

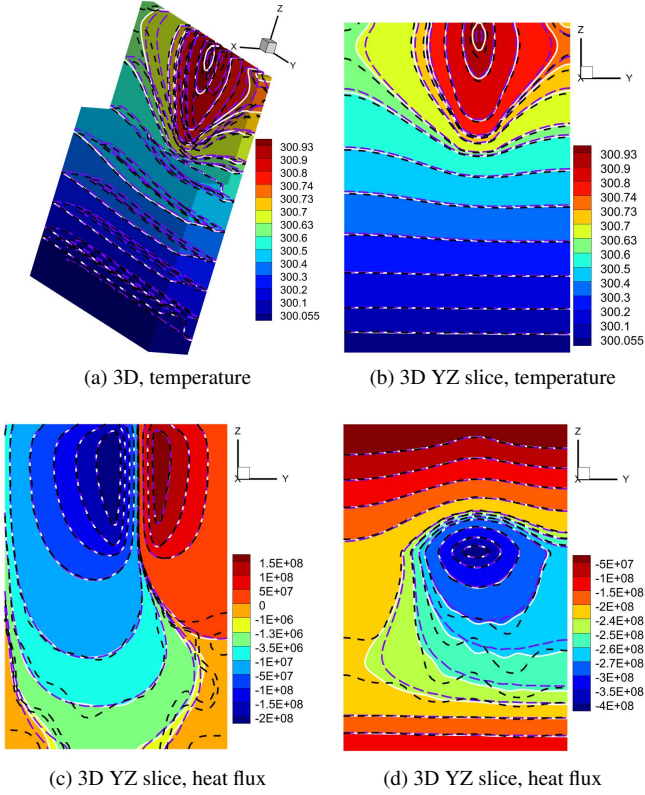


Figure B.9: (a) steady 3D temperature contour, (c,d,e) quasi-2D temperature contour, heat flux along the y and z direction in the YZ slice in the bulk FinFET (Fig. 1) with different number of discrete solid angles, where 48^2 discretized solid angles are used for colored background with white solid line, 24^2 discretized solid angles are used for black dashed line, 96^2 discretized solid angles are used for purple long dashed line.

flux contour under ‘Continuous’ heating source with different number of discrete solid angle is shown in Fig. B.9. Numerical results show that 24^2 discrete solid angles are not enough to accurately capture the non-diffusive heat conduction, and there is serious numerical jitter. Temperature fields predicted by BTE with 48^2 or 96^2 discretized solid angles are almost the same in quasi-2D simulations. Considering the huge computational amount of 3D simulation, we only use 48^2 discrete points in order to take into account both accuracy and computational efficiency.

Appendix C. Macroscopic heat diffusion equation

The macroscopic heat diffusion equation is

$$C \frac{\partial T}{\partial t} - \nabla \cdot (\kappa_{eff}(\mathbf{x}) \nabla T) = \dot{S}, \quad (C.1)$$

where effective thermal conductivity κ_{eff} in the present simulation is a scalar rather than a tensor for a given spatial position \mathbf{x} . Finite volume method is invoked and above diffusion equation in integral form over a control volume i from time t_n to

$t_{n+1} = t_n + \Delta t$ can be written as follows,

$$C_i \frac{T_i^{n+1} - T_i^n}{\Delta t} - \frac{1}{2} \sum_{j \in N(i)} S_{ij} \mathbf{n}_{ij} \cdot (\kappa_{eff}(\mathbf{x}_{ij}) \nabla T_{ij}^{n+1} + \kappa_{eff}(\mathbf{x}_{ij}) \nabla T_{ij}^n) = \frac{\dot{S}_i^n + \dot{S}_i^{n+1}}{2}, \quad (C.2)$$

$$C_i \frac{\Delta T_i^n}{\Delta t} - \frac{1}{2} \sum_{j \in N(i)} S_{ij} \mathbf{n}_{ij} \cdot (\kappa_{eff}(\mathbf{x}_{ij}) \nabla (\Delta T_{ij}^n)) = \frac{\dot{S}_i^n + \dot{S}_i^{n+1}}{2} + \sum_{j \in N(i)} S_{ij} \mathbf{n}_{ij} \cdot (\kappa_{eff}(\mathbf{x}_{ij}) \nabla T_{ij}^n), \quad (C.3)$$

where trapezoidal quadrature is used for the time integration of the diffusion and heat source terms, $\Delta T^n = T^{n+1} - T^n$, V_i is the volume of the cell i , $N(i)$ is the sets of face neighbor cells of cell i , ij is the interface between the cell i and cell j , S_{ij} is the area of the interface ij , $\kappa_{eff}(\mathbf{x}_{ij})$ is the effective thermal conductivity at the cell interface \mathbf{x}_{ij} , and \mathbf{n}_{ij} is the normal of the interface ij directing from the cell i to the cell j . Above discretizations theoretically have second-order spatial and temporal accuracy. The time step is set as $\Delta t = 0.05 t_p = 0.125$ ps and Cartesian grids with uniform cell size $\Delta x = 1$ nm is used. Conjugate gradient method is used to solve this heat diffusion equation (C.3).

To solve Eq. (C.3), one of the key input parameter is the effective thermal conductivity at the interface between medium 1 and 2. Let’s take the quasi-1D heat conduction as an example and briefly introduce how to deal with interface thermal resistance efficiently for macroscopic diffusion equation. Considering two discretized uniform cells adjacent to the interface between medium 1 and 2 with cell size Δx , as shown in Fig. A.8(c), there are different temperature distributions near the interface. The positions and temperatures of cell center are (x_1, T_1) and (x_2, T_2) , respectively. The positions and temperatures of the left and right limits of the interface are (x_L, T_L) and (x_R, T_R) , respectively, where $\Delta x/2 = x_L - x_1 = x_2 - x_R$. The heat flux at the left or right limit of the interface can be calculated based on the EFL,

$$q_1 = -\kappa_1 \frac{dT}{dx} \approx -\kappa_1 \frac{T_L - T_1}{x_L - x_1}, \quad (C.4)$$

$$q_2 = -\kappa_2 \frac{dT}{dx} \approx -\kappa_2 \frac{T_R - T_2}{x_R - x_2}. \quad (C.5)$$

The heat flux across the interface can be calculated according to the definition of interface thermal resistance,

$$q_f = \frac{T_L - T_R}{R_{eff}}, \quad (C.6)$$

where $R_{eff} = (4 - 2(t_{12} + t_{21})) / (t_{12} C_1 v_1)$ [52]. Note that the heat flux at the left or right limit of the interface and the heat flux across the interface should be equal, i.e.,

$$q_1 = q_2 = q_f. \quad (C.7)$$

Combined above four equations, we can obtain an approxi-

mated thermal conductivity κ_f at the interface,

$$q_f = -\kappa_f \frac{T_1 - T_2}{x_1 - x_2}, \quad (\text{C.8})$$

$$\kappa_f = \frac{1}{0.5/\kappa_1 + 0.5/\kappa_2 + R_{eff}/\Delta x}. \quad (\text{C.9})$$

The effective thermal conductivity in the macroscopic diffusion equation (C.1) is

$$\kappa_{eff}(\mathbf{x}) = \frac{1}{3} C v_g^2 \tau_{eff}, \quad (\text{C.10})$$

$$\tau_{eff}^{-1} = v_g/\lambda + \tau_{boundary}^{-1}, \quad (\text{C.11})$$

where the boundary scattering rate is $\tau_{boundary}^{-1} = v_g/L_{eff}$, L_{eff} is smallest characteristic length which depends on the spatial position \mathbf{x} . Specific values of L_{eff} in different spatial regions in this paper are list below. In bulk or SOI FinFET, we set $L_{eff} = 8$ nm in the fin area and $L_{eff} = 10$ nm in the bottom silicon substrate areas. In the silicon dioxide, the bulk thermal conductivity $1.4 \text{ W} \cdot \text{m}^{-1} \cdot \text{K}^{-1}$ is always used.

References

- [1] IEEE, International Roadmap for Devices and Systems (IRDS™), IEEE, 2023. URL: <https://irds.ieee.org/editions/2023>.
- [2] R. R. Das, T. R. Rajalekshmi, A. James, Finfet to gaa mbcfet: A review and insights, *IEEE Access* 12 (2024) 50556–50577. doi:10.1109/ACCESS.2024.3384428.
- [3] M. A. Alam, B. K. Mahajan, Y.-P. Chen, W. Ahn, H. Jiang, S. H. Shin, A device-to-system perspective regarding self-heating enhanced hot carrier degradation in modern field-effect transistors: A topical review, *IEEE Transactions on Electron Devices* 66 (2019) 4556–4565. doi:10.1109/TED.2019.2941445.
- [4] E. Pop, K. Goodson, Thermal phenomena in nanoscale transistors, in: *The Ninth Intersociety Conference on Thermal and Thermomechanical Phenomena In Electronic Systems (IEEE Cat. No.04CH37543)*, volume 1, 2004, pp. 1–7 Vol.1. doi:10.1109/ITHERM.2004.1319147.
- [5] Y. Qu, J. Lu, J. Li, Z. Chen, J. Zhang, C. Li, S.-W. Lee, Y. Zhao, In-situ monitoring of self-heating effect in aggressively scaled finfets and its quantitative impact on hot carrier degradation under dynamic circuit operation, in: *2020 IEEE International Reliability Physics Symposium (IRPS)*, 2020, pp. 1–6. doi:10.1109/IRPS45951.2020.9129591.
- [6] Z. W. J. Z. W. S. J. Z. Y. G. H. Ran CHENG, Bo LI, Low-temperature cmos technology for high-performance computing: development and challenges, *SCIENTIA SINICA Informationis* 54 (2024) 88–. URL: <http://www.sciengine.com/publisher/ScienceChinaPress/journal/SCIENTIASINICAInformationis/54/1/10.1360/SSI-2023-0347>. doi:https://doi.org/10.1360/SSI-2023-0347.
- [7] C. Wang, K. Vafai, Heat transfer enhancement for 3d chip thermal simulation and prediction, *Applied Thermal Engineering* 236 (2024) 121499. URL: <https://www.sciencedirect.com/science/article/pii/S1359431123015284>. doi:https://doi.org/10.1016/j.applthermaleng.2023.121499.
- [8] C. Kim, M. Lee, J. Park, J. H. Seol, Measurement and analysis of ballistic-diffusive phonon heat transport in a constrained silicon film, *Applied Thermal Engineering* 160 (2019) 114080. URL: <https://www.sciencedirect.com/science/article/pii/S1359431119307860>. doi:https://doi.org/10.1016/j.applthermaleng.2019.114080.
- [9] A. Ziabari, P. Torres, B. Vermeersch, Y. Xuan, X. Cartoixà, A. Torelló, J.-H. Bahk, Y. R. Koh, M. Parsa, P. D. Ye, F. X. Alvarez, A. Shakouri, Full-field thermal imaging of quasiballistic crosstalk reduction in nanoscale devices, *Nat. Commun.* 9 (2018) 255. URL: <https://www.nature.com/articles/s41467-017-02652-4>. doi:10.1038/s41467-017-02652-4.
- [10] X. Gu, Y. Wei, X. Yin, B. Li, R. Yang, Colloquium: phononic thermal properties of two-dimensional materials, *Rev. Mod. Phys.* 90 (2018) 041002. URL: <https://link.aps.org/doi/10.1103/RevModPhys.90.041002>. doi:10.1103/RevModPhys.90.041002.
- [11] Z. Zhang, Y. Ouyang, Y. Cheng, J. Chen, N. Li, G. Zhang, Size-dependent phononic thermal transport in low-dimensional nanomaterials, *Phys. Rep.* 860 (2020) 1–26. URL: <https://www.sciencedirect.com/science/article/pii/S0370157320300922>. doi:10.1016/j.physrep.2020.03.001.
- [12] M. A. Stettler, S. M. Cea, S. Hasan, L. Jiang, P. H. Keys, C. D. Landon, P. Marepalli, D. Pantuso, C. E. Weber, Industrial TCAD: Modeling atoms to chips, *IEEE Transactions on Electron Devices* 68 (2021) 5350–5357. doi:10.1109/TED.2021.3076976.
- [13] E. Pop, Energy dissipation and transport in nanoscale devices, *Nano Res.* 3 (2010) 147–169. URL: <https://doi.org/10.1007/s12274-010-1019-z>. doi:10.1007/s12274-010-1019-z.
- [14] S. Mishra, B. Vermeersch, V. Sankatali, H. Kukner, G. Mirabelli, F. M. Bufler, M. Brunion, D. Abdi, H. Oprins, D. Biswas, O. Zografos, F. Cathoor, P. Weckx, G. Hellings, J. Myers, J. Ryckaert, Thermal considerations for block-level ppa assessment in angstrom era: A comparison study of nanosheet fets (a10) & complementary fets (a5), in: *2024 IEEE Symposium on VLSI Technology and Circuits (VLSI Technology and Circuits)*, 2024, pp. 1–2. doi:10.1109/VLSITechnologyandCir46783.2024.10631358.
- [15] X. Chang, H. Oprins, M. Lofrano, V. Cherman, B. Vermeersch, J. D. Fortuny, S. Park, Z. Tokei, I. De Wolf, Calibrated fast thermal calculation and experimental characterization of advanced BEOL stacks, in: *2023 IEEE International Interconnect Technology Conference (IITC) and IEEE Materials for Advanced Metallization Conference (MAM)(IITC/MAM)*, 2023, pp. 1–3. doi:10.1109/IITC/MAM57687.2023.10154768.
- [16] C. Zhang, R. Guo, M. Lian, J. Shiomi, Electron–phonon coupling and non-equilibrium thermal conduction in ultra-fast heating systems, *Applied Thermal Engineering* 249 (2024) 123379. URL: <https://www.sciencedirect.com/science/article/pii/S1359431124010470>. doi:https://doi.org/10.1016/j.applthermaleng.2024.123379.
- [17] Q. Hao, H. Zhao, Y. Xiao, Q. Wang, X. Wang, Hybrid electrothermal simulation of a 3-d fin-shaped field-effect transistor based on gan nanowires, *IEEE Transactions on Electron Devices* 65 (2018) 921–927. doi:10.1109/TED.2018.2791959.
- [18] C. Landon, L. Jiang, D. Pantuso, I. Meric, K. Komeyli, J. Hicks, D. Schroeder, Localized thermal effects in gate-all-around devices, in: *2023 IEEE International Reliability Physics Symposium (IRPS)*, 2023, pp. 1–5. doi:10.1109/IRPS48203.2023.10117903.
- [19] C. Zhang, Q. Lou, H. Liang, Synthetic iterative scheme for thermal applications in hotspot systems with large temperature variance, *International Journal of Heat and Mass Transfer* 236 (2025) 126374. URL: <https://www.sciencedirect.com/science/article/pii/S0017931024012031>. doi:https://doi.org/10.1016/j.ijheatmasstransfer.2024.126374.
- [20] Y. Shen, B. Cao, Two-temperature principle for evaluating electrothermal performance of gan hemts, *Applied Physics Letters* 124 (2024) 042107. URL: <https://doi.org/10.1063/5.0189262>. doi:10.1063/5.0189262.
- [21] L. Sendra, A. Beardo, P. Torres, J. Bafaluy, F. X. Alvarez, J. Camacho, Derivation of a hydrodynamic heat equation from the phonon boltzmann equation for general semiconductors, *Phys. Rev. B* 103 (2021) L140301. URL: <https://link.aps.org/doi/10.1103/PhysRevB.103.L140301>. doi:10.1103/PhysRevB.103.L140301.
- [22] D. D. Joseph, L. Preziosi, Heat waves, *Rev. Mod. Phys.* 61 (1989) 41–73. URL: <https://link.aps.org/doi/10.1103/RevModPhys.61.41>. doi:10.1103/RevModPhys.61.41.
- [23] R. Kovács, Heat equations beyond fourier: From heat waves to thermal metamaterials, *Phys. Rep.* 1048 (2024) 1–75. URL: <https://www.sciencedirect.com/science/article/pii/S0370157323003770>. doi:https://doi.org/10.1016/j.physrep.2023.11.001.
- [24] H. Rezgui, F. Nasri, A. B. H. Ali, A. A. Guizani, Analysis of the ultrafast transient heat transport in sub 7-nm SOI FinFETs technology nodes using phonon hydrodynamic equation, *IEEE Transactions on Electron Devices* 68 (2021) 10–16. doi:10.1109/TED.2020.3039200.

- [25] C. Zhang, S. Huberman, X. Song, J. Zhao, S. Chen, L. Wu, Acceleration strategy of source iteration method for the stationary phonon boltzmann transport equation, *Int. J. Heat Mass Transfer* 217 (2023) 124715. URL: <https://www.sciencedirect.com/science/article/pii/S0017931023008608>. doi:<https://doi.org/10.1016/j.ijheatmasstransfer.2023.124715>.
- [26] S. Mazumder, Boltzmann transport equation based modeling of phonon heat conduction: Progress and challenges, *Annual Review of Heat Transfer* 24 (2022) 71–130. URL: <https://www.dl.begellhouse.com/references/5756967540dd1b03,3ae07302147f45b7,09643dee3a7e400e.html>. doi:10.1615/AnnualRevHeatTransfer.2022041316.
- [27] M. C. Barry, N. Kumar, S. Kumar, Boltzmann transport equation for thermal transport in electronic materials and devices, *Annual Review of Heat Transfer* 24 (2022) 131–172. URL: <https://dl.begellhouse.com/references/5756967540dd1b03,3ae07302147f45b7,43e971b72ed09c31.html>. doi:10.1615/AnnualRevHeatTransfer.v24.50.
- [28] Y. Hu, Y. Shen, H. Bao, Ultra-efficient and parameter-free computation of submicron thermal transport with phonon boltzmann transport equation, *Fundamental Research* 4 (2024) 907–915. URL: <https://www.sciencedirect.com/science/article/pii/S2667325822002758>. doi:<https://doi.org/10.1016/j.fmre.2022.06.007>.
- [29] A.-T. Pham, S. Jin, Y. Lu, H.-H. Park, W. Choi, M. A. Pourghaderi, J. Kim, U. Kwon, D. Kim, Simulations of self-heating effects in sige pfnfets based on self-consistent solution of carrier/phonon bte coupled system, in: 2018 International Conference on Simulation of Semiconductor Processes and Devices (SISPAD), 2018, pp. 145–148. doi:10.1109/SISPAD.2018.8551670.
- [30] M. Lofrano, H. Oprins, X. Chang, B. Vermeersch, O. V. Pedreira, A. Lesniewska, V. Cherman, I. Ciofi, K. Croes, S. Park, Z. Tokci, Towards accurate temperature prediction in BEOL for reliability assessment (invited), in: 2023 IEEE International Reliability Physics Symposium (IRPS), 2023, pp. 1–7. doi:10.1109/IRPS48203.2023.10117701.
- [31] J. Xu, Y. Hu, H. Bao, Quantitative analysis of nonequilibrium phonon transport near a nanoscale hotspot, *Phys. Rev. Appl.* 19 (2023) 014007. URL: <https://link.aps.org/doi/10.1103/PhysRevApplied.19.014007>. doi:10.1103/PhysRevApplied.19.014007.
- [32] Y. Sheng, S. Wang, Y. Hu, J. Xu, Z. Ji, H. Bao, Integrating first-principles-based Non-Fourier thermal analysis into nanoscale device simulation, *IEEE Transactions on Electron Devices* 71 (2024) 1769–1775. doi:10.1109/TED.2024.3357440.
- [33] I. N. Adisusilo, K. Kukita, Y. Kamakura, Analysis of heat conduction property in FinFETs using phonon Monte Carlo simulation, in: 2014 International Conference on Simulation of Semiconductor Processes and Devices (SISPAD), 2014, pp. 17–20. doi:10.1109/SISPAD.2014.6931552.
- [34] S. Mukhopadhyay, A. Kundu, Y. Lee, H. D. Hsieh, D. Huang, J. Horng, T. Chen, J. Lee, Y. Tsai, C. Lin, R. Lu, J. He, An unique methodology to estimate the thermal time constant and dynamic self heating impact for accurate reliability evaluation in advanced FinFET technologies, in: 2018 IEEE International Electron Devices Meeting (IEDM), 2018, pp. 17.4.1–17.4.4. doi:10.1109/IEDM.2018.8614479.
- [35] C. Zhang, L. Wu, Nonmonotonic heat dissipation phenomenon in close-packed hotspot systems, *Phys. Rev. E* 106 (2022) 014111. URL: <https://link.aps.org/doi/10.1103/PhysRevE.106.014111>. doi:10.1103/PhysRevE.106.014111.
- [36] Z. Guo, K. Xu, Discrete unified gas kinetic scheme for multiscale heat transfer based on the phonon Boltzmann transport equation, *Int. J. Heat Mass Transfer* 102 (2016) 944 – 958. URL: <http://www.sciencedirect.com/science/article/pii/S0017931016306731>. doi:10.1016/j.ijheatmasstransfer.2016.06.088.
- [37] D.-S. Tang, B.-Y. Cao, Phonon thermal transport and its tunability in GaN for near-junction thermal management of electronics: A review, *Int. J. Heat Mass Transfer* 200 (2023) 123497. URL: <https://www.sciencedirect.com/science/article/pii/S0017931022009668>. doi:<https://doi.org/10.1016/j.ijheatmasstransfer.2022.123497>.
- [38] J. Y. Murthy, S. V. J. Narumanchi, J. A. Pascual-Gutierrez, T. Wang, C. Ni, S. R. Mathur, Review of multiscale simulation in submicron heat transfer, *Int. J. Multiscale Computat. Eng.* 3 (2005) 5–32. URL: <http://dl.begellhouse.com/journals/61fd1b191cf7e96f,69f10ca36a816eb7,25fd09426d0aaf45.html>. doi:10.1615/IntJMultCompEng.v3.i1.20.
- [39] R. J. Warzoha, A. A. Wilson, B. F. Donovan, N. Donmezer, A. Giri, P. E. Hopkins, S. Choi, D. Pahinkar, J. Shi, S. Graham, Z. Tian, L. Ruppalt, Applications and impacts of nanoscale thermal transport in electronics packaging, *J Electron. Packaging* 143 (2021) 020804. URL: <https://doi.org/10.1115/1.4049293>. doi:10.1115/1.4049293.
- [40] K. Goodson, M. Flik, Effect of microscale thermal conduction on the packing limit of silicon-on-insulator electronic devices, *IEEE Transactions on Components, Hybrids, and Manufacturing Technology* 15 (1992) 715–722. doi:10.1109/33.180035.
- [41] R. Yang, G. Chen, M. Laroche, Y. Taur, Simulation of nanoscale multi-dimensional transient heat conduction problems using ballistic-diffusive equations and phonon Boltzmann equation, *J. Heat Transfer* 127 (2005) 298–306. URL: <http://dx.doi.org/10.1115/1.1857941>. doi:10.1115/1.1857941.
- [42] F. Nasri, M. Ben Aissa, H. Belmabrouk, Microscale thermal conduction based on cattaneo-vernotte model in silicon on insulator and double gate mosfets, *Applied Thermal Engineering* 76 (2015) 206–211. URL: <https://www.sciencedirect.com/science/article/pii/S1359431114010564>. doi:<https://doi.org/10.1016/j.applthermaleng.2014.11.038>.
- [43] C. Zhang, Z. Guo, Discrete unified gas kinetic scheme for multiscale heat transfer with arbitrary temperature difference, *Int. J. Heat Mass Transfer* 134 (2019) 1127–1136. URL: <http://www.sciencedirect.com/science/article/pii/S0017931018353031>. doi:10.1016/j.ijheatmasstransfer.2019.02.056.
- [44] S. Tian, T. Wu, S. Hu, D. Ma, L. Zhang, Boosting phonon transport across AlN/SiC interface by fast annealing amorphous layers, *Applied Physics Letters* 124 (2024) 042202. URL: <https://doi.org/10.1063/5.0187793>. doi:10.1063/5.0187793.
- [45] J. Chen, X. Xu, J. Zhou, B. Li, Interfacial thermal resistance: Past, present, and future, *Rev. Mod. Phys.* 94 (2022) 025002. URL: <https://link.aps.org/doi/10.1103/RevModPhys.94.025002>. doi:10.1103/RevModPhys.94.025002.
- [46] Q. Hao, H. Zhao, Y. Xiao, A hybrid simulation technique for electrothermal studies of two-dimensional GaN-on-SiC high electron mobility transistors, *J. Appl. Phys.* 121 (2017) 204501. URL: <https://doi.org/10.1063/1.4983761>. doi:10.1063/1.4983761.
- [47] M. P. Medlar, E. C. Hensel, Transient Three-Dimensional Thermal Simulation of a Fin Field-Effect Transistor With Electron-Phonon Heat Generation, Three Phonon Scattering, and Drift With Periodic Switching, *ASME Journal of Heat and Mass Transfer* 145 (2022) 022501. URL: <https://doi.org/10.1115/1.4056002>. doi:10.1115/1.4056002.
- [48] H. Honarvar, J. L. Knobloch, T. D. Frazer, B. Abad, B. McBenett, M. I. Hussein, H. C. Kapteyn, M. M. Murnane, J. N. Hernandez-Charpak, Directional thermal channeling: A phenomenon triggered by tight packing of heat sources, *Proceedings of the National Academy of Sciences* 118 (2021) e2109056118. URL: <https://www.pnas.org/doi/abs/10.1073/pnas.2109056118>. doi:10.1073/pnas.2109056118.
- [49] X. Chen, C. Hua, H. Zhang, N. K. Ravichandran, A. J. Minnich, Quasiballistic thermal transport from nanoscale heaters and the role of the spatial frequency, *Phys. Rev. Applied* 10 (2018) 054068. URL: <https://link.aps.org/doi/10.1103/PhysRevApplied.10.054068>. doi:10.1103/PhysRevApplied.10.054068.
- [50] V. A. Chhabria, S. S. Sapatnekar, Impact of self-heating on performance and reliability in finfet and gaafet designs, in: 20th International Symposium on Quality Electronic Design (ISQED), 2019, pp. 235–240. doi:10.1109/ISQED.2019.8697786.
- [51] Z. Guo, K. Xu, Progress of discrete unified gas-kinetic scheme for multiscale flows, *Adva. Aerodyn.* 3 (2021) 6. URL: <https://doi.org/10.1186/s42774-020-00058-3>. doi:10.1186/s42774-020-00058-3.
- [52] L. Zeng, G. Chen, Disparate quasiballistic heat conduction regimes from periodic heat sources on a substrate, *J. Appl. Phys.* 116 (2014) 064307. URL: <https://aip.scitation.org/doi/10.1063/1.4893299>. doi:10.1063/1.4893299.